

## RESEARCH ARTICLE

10.1002/2016JD025245

## Key Points:

- Aerosol indirect radiative effect is estimated for major cloud systems using 2B-CLDCLASS-LIDAR
- Aerosol indirect effect contributions from mixed-phase and convective clouds reduce overall forcing
- The large sensitivity and coverage of warm low-level clouds largely dominates oceanic aerosol indirect forcing

## Supporting Information:

- Supporting Information S1
- Figure S1
- Figure S2
- Figure S3
- Figure S4
- Figure S5

## Correspondence to:

M. W. Christensen,  
matthew.christensen@stfc.ac.uk

## Citation:

Christensen, M. W., Y.-C. Chen,  
and G. L. Stephens (2016), Aerosol  
indirect effect dictated by liquid  
clouds, *J. Geophys. Res. Atmos.*,  
121, doi:10.1002/2016JD025245.

Received 17 APR 2016

Accepted 1 DEC 2016

Accepted article online 9 DEC 2016

## Aerosol indirect effect dictated by liquid clouds

Matthew W. Christensen<sup>1</sup>, Yi-Chun Chen<sup>2</sup>, and Graeme L. Stephens<sup>2</sup>
<sup>1</sup>Department of Atmospheric Sciences, Colorado State University, Fort Collins, Colorado, USA, <sup>2</sup>Jet Propulsion Laboratory, California Institute of Technology, Pasadena, California, USA

**Abstract** Anthropogenic aerosols have been shown to enhance the solar reflection from warm liquid clouds and mask part of the warming due to the buildup of greenhouse gases. However, very little is known about the effects of aerosol on mixed-phase stratiform clouds as well as other cloud regimes including cumulus, altocumulus, nimbostratus, deep convection, and anvil cirrus. These additional cloud categories are ubiquitous and typically overlooked in satellite-based assessments of the global aerosol indirect forcing. Here we provide their contribution to the aerosol indirect forcing estimate using satellite data collected from several colocated sensors in the A-train for the period 2006–2010. Cloud type is determined according to the 2B-CLDCLASS-LIDAR CloudSat product, and the observations are matched to the radiative flux measurements from CERES (Clouds and the Earth's Radiant Energy System) and aerosol retrievals from MODIS (MODerate resolution Imaging Spectroradiometer). The oceanic mean aerosol indirect forcing is estimated to be  $-0.20 \pm 0.31 \text{ W m}^{-2}$  with warm low-level cloud largely dictating the strength of the response ( $-0.36 \pm 0.21 \text{ W m}^{-2}$ ) due to their abundance and strong cloud albedo effect. Contributions from mixed-phase low-level cloud ( $0.01 \pm 0.06 \text{ W m}^{-2}$ ) and convective cloud ( $0.15 \pm 0.23 \text{ W m}^{-2}$ ) are positive and buffer the system due to strong aerosol-cloud feedbacks that reduce the cloud albedo effect and/or lead to convective invigoration causing a countering positive longwave warming response. By combining all major cloud categories together, aerosol indirect forcing decreases and now contains positive values in the uncertainty estimate.

## 1. Introduction

Anthropogenic aerosol emissions can affect the radiative properties of clouds and possibly climate. Aerosol indirect effects impose one of the largest sources of uncertainty in projecting climate change [Intergovernmental Panel on Climate Change (IPCC), 2013]. The uncertainty stems from a myriad of cloud feedbacks that can act to enhance or diminish the strength of the aerosol indirect effect. These feedbacks are poorly represented in models [e.g., Golaz et al., 2013] and have been shown to depend on many parameters such as cloud type and meteorology [Khain, 2009].

Reported values of the global aerosol indirect forcing estimate have traditionally stemmed solely from the observations of warm liquid clouds [e.g., Lebsock et al., 2008; Quaas et al., 2008; Chen et al., 2014] and excluding other, possibly important, cloud systems (e.g., deep convective clouds) from the overall estimation. Warm low clouds are commonly isolated because many of the assumptions (e.g., plane parallel clouds with spherical cloud drops) used in the radiative transfer computations are reasonable, and, thus, the retrieved properties tend to be well constrained (with relatively low uncertainty). The extent to which other cloud types (for example, low-level mixed-phase clouds) contribute to the indirect forcing estimation is essentially unknown or poorly understood from limited studies. While warm low clouds offer great opportunities to untangle aerosol-cloud interactions due to their sheer abundance and impact on cloud radiative forcing, it may be imperative to analyze all major cloud systems that could potentially buffer or enhance the global aerosol indirect forcing estimate. With the recent advances in spaceborne satellite instrumentation (e.g., the addition of radar and lidar active sensors) these assessments can be reliably extended to mixed-phase clouds.

In warm clouds an increase in aerosol concentration typically decreases cloud droplet size and increases droplet concentration [Twomey, 1974]. This process can lead to suppression of precipitation [Albrecht, 1989] causing an increase in cloud water path, depth, fraction, and albedo [Pincus and Baker, 1994]. However, the strength of the indirect effect in warm clouds also critically depends on meteorological conditions. Principally, free-troposphere humidity and lower troposphere stability play prominent roles in affecting the magnitude

and sign of the response [e.g., see *Ackerman et al.*, 2004; *Chen et al.*, 2014]. An increase in cloud albedo results in more reflected sunlight to space thereby exerting a cooling influence on the Earth's surface. The radiative forcing attached to aerosol-cloud interactions is estimated to be  $-0.45 \text{ W m}^{-2}$  with an uncertainty range of  $-1.2$  to  $0 \text{ W m}^{-2}$  [IPCC, 2013, chapter 7]. This (most recent) estimate has decreased considerably in magnitude from the previous IPCC Fourth Assessment Report (reported value of  $-0.78 \text{ W m}^{-2}$  [IPCC, 2007]) due to more of the models including aerosol-mixed-phase and convective cloud parameterization schemes in the computation of the radiative forcing.

In mixed-phase clouds the interactions between aerosols, cloud droplets, and ice particles add a deeper level of complexity and uncertainty due to many more aerosol-related cloud feedbacks. Three prominent aerosol indirect effect mechanisms have been identified in mixed-phase clouds: the riming indirect effect (increase in cloud condensation nuclei (CCN) decreases riming and precipitation causing more reflective clouds) [Borys et al., 2003], the glaciation indirect effect (increase in ice nuclei enhances ice production and precipitation causing fewer and less reflective clouds) [Lohmann, 2002], and the convective invigoration effect (increase in aerosol delays the onset of precipitation causing more release of latent heat higher in the cloud which promotes stronger vertical updrafts and deeper clouds) [Rosenfeld et al., 2008] all of which are nonlinearly affected by meteorology.

For mixed-phase low clouds capped by a strong temperature inversion (e.g., those commonly found in the Arctic) the first two stated processes are likely to have the most relevance since the convective invigoration mechanism is inhibited by strong temperature inversions above the boundary layer [Rosenfeld et al., 2013]. Recent ship track observations of mixed-phase clouds capped by a strong inversion demonstrate that the cloud albedo effect is significantly suppressed due to a substantial loss of total cloud water in polluted clouds [Christensen et al., 2014]. By contrast, ground-based sites across the Arctic reveal that increased anthropogenic aerosol actually enhance cloud water path and coverage (possibly via the riming indirect effect) thereby causing greater shortwave cooling in summer but stronger infrared warming during winter [Garrett et al., 2002]. Overall, it remains unclear how clouds respond to elevated levels of aerosol in high latitudes, and, as a result, studies have varying degrees of strength and even signs of the aerosol indirect forcing estimate. Values range between  $-0.98 \text{ W m}^{-2}$  and  $0.12 \text{ W m}^{-2}$  over the Arctic Ocean [e.g., see *Alterskjær et al.*, 2010].

In free-tropospheric clouds under relatively weak temperature inversions aerosol can invigorate convection thereby leading to higher cloud tops [Storer et al., 2014] and more expansive anvils [Fan et al., 2013]. The aerosol invigoration effect increases cloud depth and cloud reflectivity (cooling effect) while at the same time increasing cloud height and decreasing the outgoing longwave radiation flux (warming effect). As a consequence, the shortwave and longwave radiative fluxes tend to oppose each other and the forcing can actually be positive (especially at night) due to the strong longwave warming influence by spreading anvils. The opposing longwave and shortwave radiative effects have been studied for convective clouds although only over remote continental and maritime locations [e.g., see *Fan et al.*, 2013]. The extent to which aerosol influences convective clouds on the global scale are of great interest for understanding total aerosol indirect forcing.

Meteorology also plays a vital role on the aerosol response in convective clouds. Differing cloud feedbacks that lead to opposite aerosol-convective cloud interactions have been shown to arise under certain meteorological conditions. For example, polluted convective clouds can entrain more dry air causing them to desiccate in a relatively high wind shear environment particularly in the midlatitudes [Fan et al., 2009]. For that reason we examine the influence of meteorology on the aerosol indirect effect response and attempt to estimate the globally averaged indirect forcing for tropical and midlatitude convective clouds separately.

Several questions are posed in this research:

1. How much of the Earth's ocean surface is covered by warm low-level cloud, mixed-phase low cloud, and convective cloud?
2. What is the indirect effect sensitivity for each of these cloud regimes to increased concentration of aerosols?
3. What contribution does each cloud system make to the oceanic averaged aerosol indirect forcing estimate?

## 2. Data and Methodology

### 2.1. Data

Data collected in this study are obtained from multiple sensors throughout the constellation of A-Train satellites. We utilize two active sensors, the 94 GHz cloud profiling radar (CPR) on CloudSat and the 532 nm lidar on CALIPSO (Cloud-Aerosol Lidar and Infrared Pathfinder Satellite Observations), and two passive sensors, the MODIS (MODERate resolution Imaging Spectroradiometer) and CERES (Clouds and the Earth's Radiant Energy System) instruments on the Aqua satellite. Aerosol optical thickness is acquired from three data sets: the MODIS level 3 gridded product (MYD08), MACC (Monitoring Atmospheric Composition and Climate) reanalysis product, and CALIPSO level 2 product.

Cloud top and bottom temperatures are obtained by interpolation of the cloud layer altitude (obtained from 2B-CLDCLASS-LIDAR) with the vertical temperature profile from ECMWF (European Centre for Medium-Range Weather Forecasts) Auxiliary matched CloudSat product. Because cloud base temperature is not a standard MODIS cloud retrieval, the ECMWF-AUX temperature profile is used for consistency to select the temperature at both cloud top height and bottom. The differences in cloud top temperature between the MODIS standard collection 6 product and the interpolated estimate with ECMWF-AUX used here is less than 0.3 K when averaged globally across boundary layer cloud types. Cloud effective radius and optical thickness are obtained from the MODIS level 2 product (MYD06). For warm clouds the estimated uncertainty on the effective radius retrieval is approximately 30% [Bennartz, 2007]. Cloud albedo and top of atmosphere radiative fluxes are examined using the CERES CALIPSO CloudSat MODIS (CCCM) product [Kato *et al.*, 2010] that provides measured fluxes over the 20 km CERES footprint to an accuracy of approximately 1% globally averaged [Loeb *et al.*, 2009].

Aerosol optical depth is obtained from MODIS level 3 data, which are a column-integrated quantity produced from level 2 retrievals at a nominal spatial resolution of 10 km, then averaged over  $1^\circ \times 1^\circ$  grid cells. The size of the grid is large enough to include a sufficient number of samples to regress the MODIS 1 km retrievals of cloud onto the aerosol but small enough to avoid significant spatial variations in aerosol optical depth that extend beyond this spatial scale [Anderson *et al.*, 2003].

The sampling strategy used in this study is the same as that described in Chen *et al.* [2014]; we collocate all of the satellite observations and reanalysis products to the CloudSat ground track. This approach allows us to examine the MODIS cloud properties (at 1 km resolution) and CERES radiative fluxes (at 20 km resolution) alongside aerosol optical depth retrievals that are averaged over larger  $1^\circ$  gridded regions. While this minimizes the standard satellite problem of retrieving aerosol and cloud together, the tradeoff is that this approach may introduce computational biases related to the varying averaging spatial scales of each data product [McComiskey and Feingold, 2012]. The effect of spatial resolution typically decreases the strength of the cloud albedo effect as the sensor footprint becomes larger. These concerns were addressed in Chen *et al.* [2014] in which the spatial-scale resolution biases relating varying footprint sizes of the various satellite products were found to have a relatively small impact on the cloud albedo effect; we refer interested readers to the stated paper.

### 2.2. Satellite Retrieval Artifacts

Many of the challenges related to the retrieval of aerosol properties have remained significant despite decades of progress in technological advancements and analysis methods. The uncertainty in retrieved aerosol optical depth is related to several well-known factors including cloud contamination (artificially high aerosol optical depth (AOD) retrieval due to the presence of cloud particles undetected by the sensor in cloud-free areas), 3-D effects in broken cloud systems (erroneously high AOD retrievals due to scattering of light by inhomogeneous clouds), relative humidity (falsely enhanced AOD signal due to hygroscopic growth by humidity), near-surface wind speed (sea surface brightness contamination causing artificially high AOD), and wet scavenging (lack of satellite-retrieved AOD in heavily precipitating clouds), to name a few [e.g., see Grandey *et al.*, 2013].

Throughout the analysis attempts are made to limit the uncertainty related to some of these factors. We use the standard MODIS (MYD04) aerosol product that averages the 1 km pixel retrievals over larger 10 km clustered regions to limit cloud contamination. This is accomplished in the MYD04 product by selecting only those pixels deemed as confidently cloud-free by eliminating the darkest and brightest 25% of each cluster [Remer *et al.*, 2005]. Nevertheless, despite these considerations the MODIS AOD retrieval may contain some residual artifacts introduced by clouds and the above mentioned factors may lead to biases and/or spurious relationships in some of the regressions derived between the retrieved cloud properties and aerosol optical depth

[Grandey *et al.*, 2013] particularly for deep convective clouds where wet scavenging likely influences aerosol concentrations [Koren *et al.*, 2010].

Convective clouds can transport aerosol from the surface into the upper troposphere [Pueschel *et al.*, 1997]. They can also remove aerosol through wet scavenging and cloud nucleation. Low aerosol concentrations are often retrieved in cloud-free air near deep convective polluted clouds due to the scavenging effect. It is noteworthy that this effect may lead to spurious aerosol-precipitation relationships [Grandey *et al.*, 2013] thereby making the assessment difficult to quantify interactions in deep convective clouds. Other studies have avoided this issue by selecting aerosol measurements in the vicinity of clouds prior to the onset of precipitation [e.g., see Sorooshian *et al.*, 2009]. However, untangling these effects from the analysis cannot be completely achieved from the measurements used here since we cannot retrieve aerosol beneath clouds, and therefore, we cannot rule out any influence of a scavenging effect on the analysis. These inherent uncertainties pose significant challenges to the accurate estimation of the aerosol indirect forcing. Because it is not the intended purpose of this work to evaluate the intrinsic uncertainty of the aerosol-precipitation retrieval, we take a conservative screening approach to limit its influence on the presented results.

### 2.3. Screening Method and Aerosol Proxy

Several precautions are taken to limit artifacts in the retrieval of aerosol and cloud. The retrieved optical properties of clouds become less accurate if either an overlying thin cloud or aerosol layer is present. These conditions are removed using the lidar on CALIPSO. An overlying layer of aerosol can introduce semidirect effects [Wilcox, 2010] and increase the uncertainty of the cloud retrieval. Furthermore, cloud retrievals tend to become more uncertain due to 3-D and shadow effects caused by steep solar zenith angles. Therefore, we only select satellite observations with low solar zenith angle (less than 65°) to limit some of these potential biases. The satellite data collected and screened using these colocated sensors in the A-train during the period 2006–2010 provided 6.75 million profiles to quantify aerosol indirect forcing.

This study uses aerosol index ( $AI = \tau \times \text{\AA}$ , where  $\tau$  is the aerosol optical depth at 550 nm and  $\text{\AA}$  is the Ångström exponent derived from the optical depths at 550 nm and 875 nm) derived from MODIS data as a proxy for column cloud condensation nuclei (CCN). Aerosol index has been shown to serve as a better indicator of the column CCN than AOD [Nakajima *et al.*, 2001] because the size of the aerosol particles is inversely proportional to the Ångström exponent thereby giving more weight to the fine-mode aerosols. Calculations based on the aerosol optical depth proxy have also been carried out in this research to examine parametric uncertainty (additional information is described in Text S4 in the supporting information).

### 2.4. Cloud Classification

The CloudSat radar retrieves a vertical profile (at 240 m vertical resolution) of reflectivity ( $Z_e$ ) and converts this information to obtain a path-integrated attenuation, geometric thickness of cloud, and surface precipitation rate [Haynes *et al.*, 2009]. We exploit the synergy between the radar and CALIPSO lidar to retrieve the vertical and horizontal structure of clouds. The radar has the ability to probe through optically thick cloud layers (like convection), while the lidar can easily observe tenuous clouds (like cirrus) and low-level boundary clouds which the radar frequently misses [Christensen *et al.*, 2013]. These data sets are merged together along the CloudSat ground track to form the 2B-GEOPROF-LIDAR product. Clouds are grouped into cloud types (i.e., cirrus, alto stratus, alto cumulus, stratus, stratocumulus, cumulus, nimbostratus, and deep convective) using a detection algorithm [Wang and Sassen, 2001] in the 2B-CLDCCLASS-LIDAR product. The algorithm categorizes the cloud type based on some basic features (e.g., cloud top/base layer altitude, horizontal extent, and precipitation) of the major cloud types [World Meteorological Organization, 1956]. The distribution of each cloud type is in general agreement with observations from the International Satellite Cloud Climatology Project (ISCCP) and surface observer reports [Li *et al.*, 2015].

Figure 1 is a particular example of the various cloud types identified in a weather system extending from the tropics to the midlatitudes on 27 March 2008. The 11  $\mu\text{m}$  MODIS imagery is used to highlight the contrast between high- (bright white) and low-level cloud tops (gray). The ground track of CloudSat and CALIPSO is superimposed onto the MODIS imagery. Vertical profiles through each cloud type are shown in the portion of the ground track in Figures 1a–1c. Annual mean distributions of each cloud type are shown in Figure 2 (and Figure S1 for individual cloud type regimes). Cumulus and deep convective clouds are vertically developed and tend to reside in the tropics, while stratus and stratocumulus predominately reside in subtropical regions. Nimbostratus clouds, commonly found in midlatitude storm tracks and occasionally in the ITCZ (Intertropical Convergence Zone), are horizontally and vertically extensive. Altostratus and altocumulus clouds are tall with



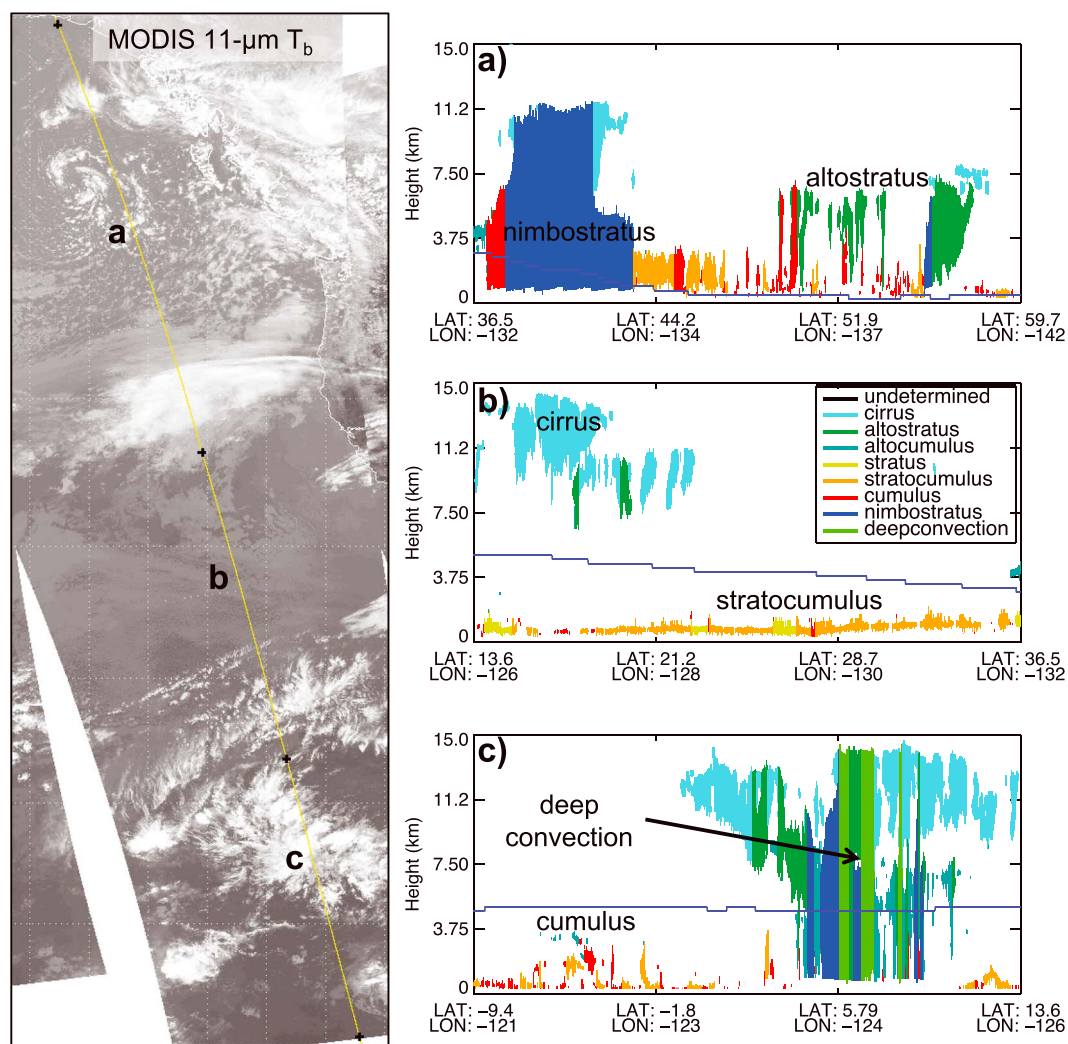


**Figure 1.** (left) Brightness temperature (T<sub>b</sub>) of MODIS 11 μm imagery shows several distinct cloud systems to the west of North America on 27 March 2008 at approximately 2130 UTC. Colder brightness temperatures are bright white, while warmer temperatures are dark as represented on a gray scale. (a–c) Clouds are extracted and classified into segments along the CloudSat-CALIPSO track (yellow line) using the 2B-CLDCLASS-LIDAR product. Blue solid line indicates the height of the melting level as determined from ECMWF ERA-Interim data.

relatively high and variable cloud base heights ranging from 2 to 7 km. They are also commonly identified in the vicinity of deep convective clouds and in the storm tracks of midlatitude cyclones. Cirrus clouds tend to have the highest cloud bases and are excluded from this analysis since they do not directly interact with anthropogenic aerosol produced near the surface (see section 3.4 for details). Cirrus that is detected within 150 km of either a deep convective or nimbostratus cloud using CloudSat is labeled as “anvil cirrus” and included in the analysis since it probably interacts with the local aerosol. Anvil cirrus clouds typically form from the detrainment of deep convective clouds near the level of the tropopause. Concentrations of aerosols in anvil cirrus are about 4 times larger than the background air due to the outflow from deep convection [Pueschel *et al.*, 1997]. The frequency of anvil cirrus detected here, however, is likely underestimated due to CloudSat’s limited sampling capabilities and is used here anyway to understand the response to elevated concentrations of aerosols.

### 2.5. Indirect Radiative Forcing

The general approach to estimate the aerosol indirect radiative forcing involves four steps: (1) single-layer clouds are selected and grouped by cloud type (e.g., warm low cloud, cold low cloud, and convective cloud) using the 2B-CLDCLASS-LIDAR product, (2) ocean mean sensitivities are calculated from the linear regression

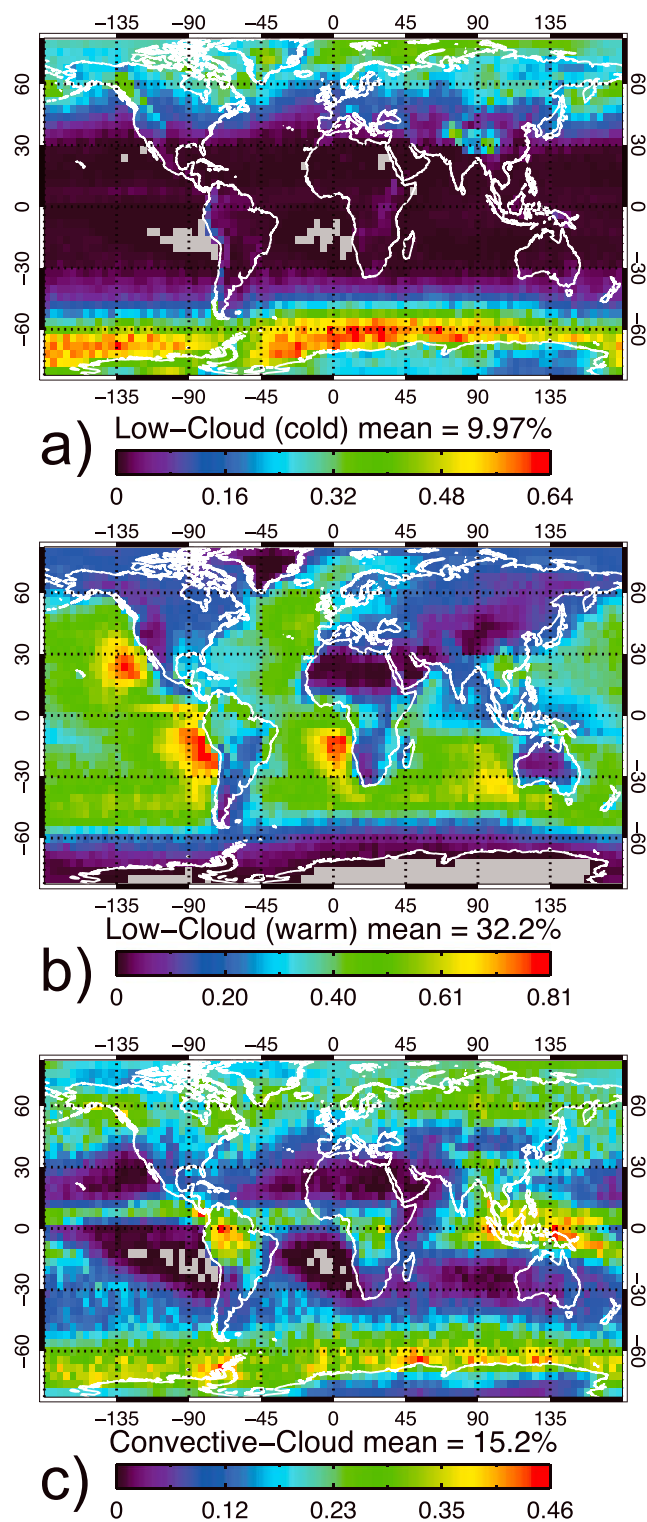


**Figure 2.** Annual mean oceanic distributions of (a) cold low clouds, (b) warm low clouds, and (c) convective clouds using the 2B-CLDCLASS-LIDAR product. Means are constructed from CloudSat profiles selected inside  $4^\circ \times 4^\circ$  regions. Low clouds consist of stratus, stratocumulus, and cumulus. Convective clouds consist of altostratus, nimbostratus, and deep convection, all with cloud base heights below 2 km, and anvil cirrus. Composites for individual cloud types are displayed in Figure S1. Cloud top temperature is derived by interpolating the CALIOP cloud top height to the ECMWF-AUX vertical temperature profile and considered cold (warm) if the temperature is below (above)  $-5^\circ\text{C}$ .

between the top of atmosphere CERES radiative flux and MODIS *AI* for the selection of single-layer clouds over the globe, (3) all-sky cloud fraction ( $\overline{c_m}$ ) is gridded for each category, and (4) the annual mean anthropogenic aerosol fraction is computed from MACC-II reanalysis data. Finally, the radiative forcing is computed from the product of the aerosol indirect effect sensitivity, cloud fraction, and anthropogenic aerosol fraction over each  $4^\circ \times 4^\circ$  region.

To estimate the indirect effect at the top of the atmosphere, we quantify the sensitivity of the cloud radiative effect

$$C_{SW,LW} = F_{CLR} - F_{OBS} \quad (1)$$

to variations in aerosol optical depth for shortwave ( $C_{SW}$ ) and longwave ( $C_{LW}$ ) components of the radiation flux where,  $F_{CLR}$  is the clear-sky net radiative flux (i.e.,  $F_{CLR} = F_{CLR}^{\uparrow} - F_{CLR}^{\downarrow}$ , arrows denote upwelling and downwelling fluxes, respectively), and  $F_{OBS}$  is the all-sky radiative flux. To isolate the clear-sky area within the CERES field of view,  $F_{OBS}$  can be decomposed into

$$F_{OBS} = (1 - c_f)F_{CLR} + c_f F_{CLD}, \quad (2)$$

where clear-sky and cloud sky ( $F_{CLD}$ ) radiative fluxes are computed from the cloud cover fraction ( $c_f$ ) using MODIS 1 km data. Clear-sky fluxes are obtained from the CCCM product and constrained against top of atmosphere measurements using a radiative transfer model that accounts for the surface roughness and atmospheric temperature and humidity for each CERES pixel [e.g., see Kato *et al.*, 2011; Fu and Liou, 1993; Stephens *et al.*, 1991; Jin *et al.*, 2011; Wilber *et al.*, 1999] (supporting information Text S5). Taking the derivative of the TOA cloud radiative forcing (equation (1)) with respect to aerosol index (*AI*) and combining it with equation (2) gives

$$\frac{dC_{SW,LW}}{d \ln AI} = \left( \overline{c_m} \left[ \frac{dF_{CLR}}{d \ln AI} - \frac{dF_{CLD}}{d \ln AI} \right] + (F_{CLR} - F_{CLD}) \frac{dc_f}{d \ln AI} \right), \quad (3)$$

where  $\overline{c_m}$  is the grid box mean cloud fraction determined using 2B-CLDCLASS-LIDAR cloud mask and  $c_f$  is the MODIS cloud fraction averaged over the CERES footprint and is used to derive cloud albedo for shortwave calculations. The number of samples globally available to compute  $c_f$  is smaller than in  $\overline{c_m}$  due to the screening protocols and occasional retrieval failures of clouds in the MODIS product. To limit potential sampling biases, a climatological cloud fraction  $c_m$  value is used to weight the first term in equation (3) instead of using  $c_f$  which would give a lower value of the cloud fraction estimate. The first term is the intrinsic aerosol indirect effect, which accounts for the impact of aerosol changes on cloud albedo, and the second term is the extrinsic aerosol indirect effect, expressing the impact of aerosol on cloud fraction. Due to known biases and large uncertainties related to the systematic positive relationship between cloud cover fraction and aerosol optical depth, we do not assess the impact of it here and recommend the results presented in Gryspeerdt *et al.* [2016] and Chen *et al.* [2014].

To estimate the indirect radiative forcing (IRF), equation (3) is multiplied by the increase in aerosols attributed to anthropogenic activities

$$IRF = \frac{dC_{SW,LW}}{d \ln AI} \frac{d \ln AI}{d \ln \tau_a} \Delta \tau_a, \quad (4)$$

where,  $\Delta \tau_a$  is the increase in aerosol optical ( $\tau_a$ ) due to anthropogenic activities which can be expressed as

$$\Delta \tau_a = \ln(\tau_a) - \ln(\tau_a - \tau_{anth}) = \ln \left( \frac{1}{1 - F_{anth}} \right), \quad (5)$$

where,  $\tau_{anth}$  is the anthropogenic aerosol optical depth, and  $F_{anth}$  is the anthropogenic aerosol fraction. The MACC-II product provides an estimate of the total and anthropogenic part of the aerosol optical depth and can thus be used to infer the fraction of the total aerosol that may be considered anthropogenic following the method outlined in Bellouin *et al.* [2013]. The first derivative term in equation (4) is the sensitivity of cloud radiative forcing to changes in aerosol index and is obtained from equation (3). The second derivative term in equation (4) is the sensitivity of *AI* to a relative change in aerosol optical depth ( $\tau_a$ ) used to relate aerosol index to aerosol optical depth. On average the linear regression and correlation coefficients of  $\frac{d \ln AI}{d \ln \tau_a}$  are 0.85 and 0.67, respectively and the regression coefficient is statistically significant using a two-tailed *T* test for oceanic regions used here. The error propagated by this term increases the relative uncertainty by approximately 15%.

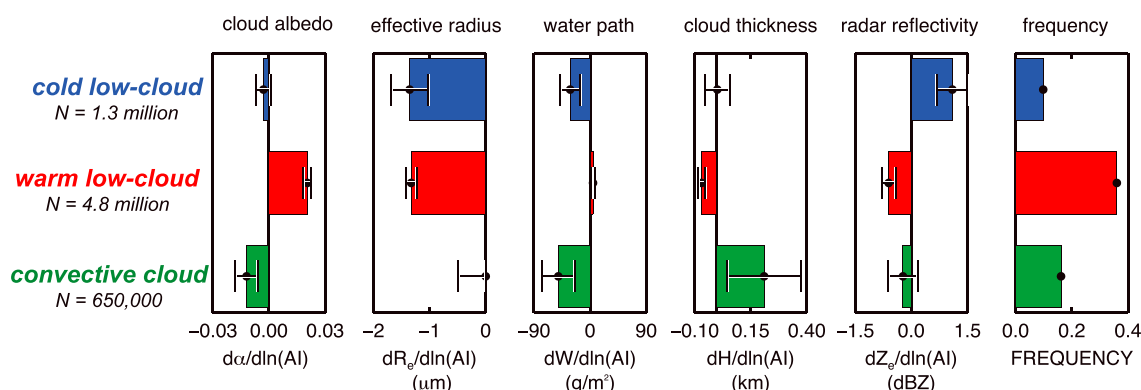


**Figure 3.** Observed sensitivity of cloud albedo derived using CERES ( $\alpha$ ), MODIS effective radius ( $R_e$ ), total water path ( $W$ ), CloudSat/CALIPSO cloud depth ( $H$ ), radar reflectivity ( $Z_e$ ), and relative frequency of occurrence (FREQUENCY) as a function of aerosol index ( $AI$ ) for each major cloud category. Analysis is based on millions of profiles ( $N$ ) taken from observations over the global oceans during the period from June 2006 to December 2010. The uncertainty is expressed as a  $1\sigma$  error on the regression. Cloud categories are classified using the 2B-CLDCLASS-LIDAR product as low-level cloud (combined layers of stratus, stratocumulus, and cumulus) having warm and cold cloud top and convective cloud (combined layers of altocumulus, altostratus, nimbostratus, deep convection, and anvil cirrus). Cloud top temperature is considered cold (warm) if the temperature is below (above)  $-5^\circ\text{C}$ .

MACC-II is a satellite-model hybrid data set that utilizes the state-of-the-art ECMWF-IFS (Integrated Forecast System) aerosol transport model along with a surface emissions inventory and assimilated MODIS data to provide aerosol optical depth for a variety of species including dust, organic carbon, sea salt, black carbon, and sulfate (e.g., see Morcrette *et al.* [2009] and Benedetti *et al.* [2009] for details). MACC-II reanalysis data are used to extract  $F_{\text{anth}}$  from several AOD species using the method outlined in Bellouin *et al.* [2013]. The global distribution of the anthropogenic aerosol fraction is shown in Figure S4. The global mean value we obtain using MACC-II data is 0.215 and similar to estimates derived in other studies [Kaufman *et al.*, 2005; Bellouin *et al.*, 2013].

Overall, the aerosol indirect radiative forcing is a strong function of the cloud fraction, cloud albedo sensitivity to changes in aerosol, cloud fraction sensitivity to changes in aerosol (not evaluated here), and the increase in aerosols attributed to anthropogenic activities ( $\Delta\tau_a$ ). The shortwave intrinsic indirect effect is primarily governed by the cloud albedo effect but can be decomposed further into sensitivities involving effective radius, total water path, and cloud depth changes to increasing aerosol index. For shortwave calculations the fluxes are obtained from the product of the instantaneous CERES albedo measurements multiplied by the annual mean incoming solar radiation flux ( $\overline{F^{\downarrow}}$ ) which is computed following the method outlined in Coakley [1979].

### 3. Results

The aerosol indirect effect is estimated separately for warm and cold-topped boundary layer clouds. For this study, boundary layer clouds consist of stratus, stratocumulus, and cumulus. Convective clouds consist of altocumulus, altostratus, nimbostratus, deep convection, and anvil cirrus. Anvil cirrus is included if a convective core is located within 300 km of the observed cirrus cloud. While warm topped convective clouds are rare, they are included in the convective cloud composite.

#### 3.1. Boundary Layer Clouds

Boundary layer clouds are ubiquitous and cover approximately 40% of the global ocean (see Figure 2 and Figure S1); consistent with Wood [2012]. Interestingly, cold/mixed-phase clouds (cloud top temperature less than  $-5^\circ\text{C}$ ) make up a substantial portion (about one third) of all boundary layer clouds. Due to their abundant coverage, it is thus imperative to incorporate their radiative signature in aerosol indirect effect studies.

The mean oceanic aerosol indirect effect sensitivities are calculated and shown in Figures 3 and S2 for a variety of cloud properties. Here we find general agreement with previous satellite-based assessments of aerosol effects on warm clouds, e.g., cloud albedo (effective radius) increases (decreases) with  $AI$ . By contrast, the cloud albedo effect is significantly weaker when the boundary layer cloud tops are cold. The weaker response coincides with concurrent decreases in total water path and increases in precipitation.

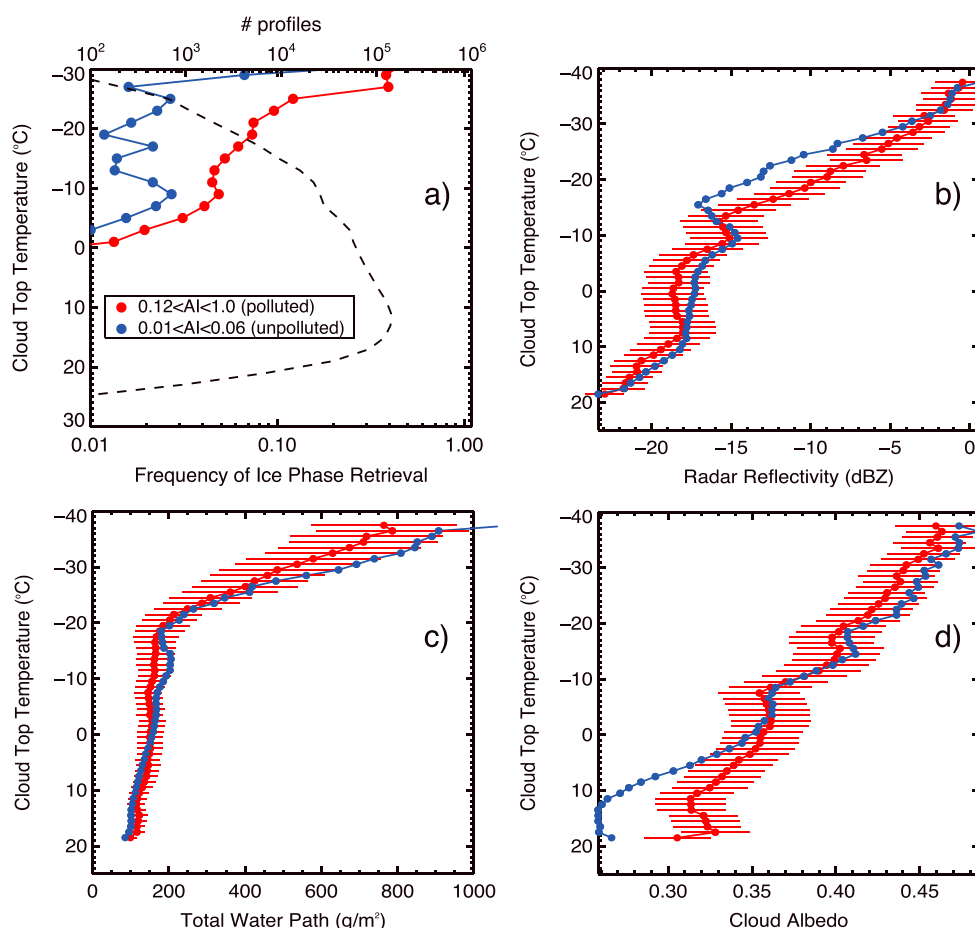


**Figure 4.** Binned averages of (a) ice phase occurrence (CloudSat/CALIPSO), (b) radar reflectivity (CloudSat), (c) total water path (MODIS), and (d) all-sky albedo (CERES) as a function of CALIPSO cloud top temperature for cloud layers classified as either stratocumulus, or cumulus in the 2B-CLDCLASS-LIDAR product. Data are grouped into 1°C wide bins for polluted (red line) and unpolluted (blue line) conditions. Atmosphere is considered polluted or unpolluted based on the aerosol index range specified on the legend. Total number of CloudSat profiles for each bin in Figure 4a is displayed as the dashed line. Cloud phase retrievals are normalized so the percentages of each category (water, ice, and mixed) sum to 100%; the ice and mixed categories are combined and displayed. Error bars (Figures 4b–4d) denote the 5–95% confidence interval.

To understand this response, cloud albedo for cold-topped boundary layer clouds is examined as a function of cloud top temperature. Observations are grouped separately in Figure 4 for clean ( $0.01 < AI < 0.06$ ) and polluted ( $0.12 < AI < 1$ ) conditions. This range was chosen to provide roughly an equal weighting of samples for polluted and clean conditions. Evidently, the cloud albedo effect is largest when the cloud tops are warm and the response gradually decreases with decreasing temperature. Astoundingly, the cloud albedo effect reverses at approximately  $-5^{\circ}\text{C}$  where further cooling leads to more aggressive cloud dimming by increasing  $AI$ , although with less statistical confidence. The signature of this response can be understood via the glaciation aerosol indirect effect mechanism, in which more aerosol and presumably ice nuclei promotes larger ice crystal concentrations (Figure 4a) and heavier precipitation in mixed-phase boundary layer clouds thereby causing them to lose more total water and reflect less solar radiation [Christensen et al., 2014]. The CloudSat radar (being sensitive to precipitation sized particles) identifies larger radar reflectivity, and hence heavier precipitation, in polluted mixed-phase clouds compared to unpolluted clouds (Figure 4b). Also, the radar detects lighter precipitation in warm phase clouds when they are polluted on average. Based on these aerosol-cloud sensitivities, we do not expect anthropogenic aerosol to have a substantial effect on the shortwave albedo of mixed-phase stratocumulus cloud in the Arctic.



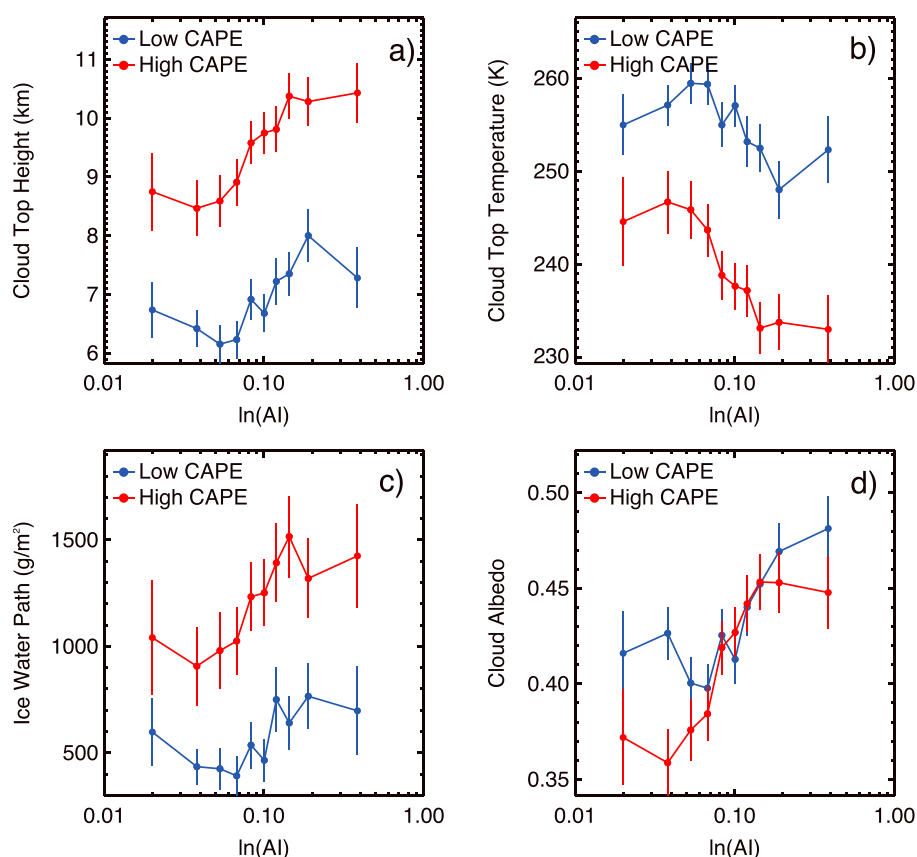


**Figure 5.** Mean (a) cloud top height (CALIOP), (b) cloud top temperature (CALIOP), (c) ice water path (CloudSat) and (d) cloud albedo (CERES) binned by aerosol index (MODIS) and composited by low/high values of CAPE for convective clouds in the tropics (30°S–30°N). Low CAPE is defined here as a value less than 100 J/kg. Widths of bins are constructed to contain roughly the same number of samples for each average. Error bars denote the 5–95% confidence interval.

### 3.2. Convective Clouds

Convective free-troposphere clouds (as defined in this study) cover approximately 14% of the global oceans (8% in the midlatitudes and 6% in the tropics, e.g., see Figures 2 and S1). Strong cloud top height ( $\frac{dH}{d \ln AI}$ ) and modest cloud albedo ( $\frac{dA}{d \ln AI}$ ) indirect effect sensitivities are observed in convective clouds (Figure 5) in the tropics (30°S–30°N latitude). These sensitivities are similar for levels of low and high CAPE (convective available potential energy). The calculation of CAPE follows from the vertical profiles of temperature and humidity provided by the ECMWF-AUX product. Figure 5 shows several convective cloud properties binned by AI. The strong increase in cloud top height with AI implies that the net effect of increasing aerosols is to invigorate deep convection. This is consistent with the results from many studies [e.g., Rosenfeld *et al.*, 2008; Fan *et al.*, 2009, 2013; Storer *et al.*, 2014; Gryspeerd *et al.*, 2014]. The deeper convective clouds at higher AI have colder cloud tops (Figure 5b) and larger ice/total water paths (Figure 5c). As a consequence, aerosol effects on tropical deep convective cloud lead to higher cloud albedo (Figure 5d) and less cloud top longwave emission.

On the other hand, these responses tend to be opposite and nonlinear (e.g., the reversal of cloud top height/temperature trends at moderate AI) in the extratropics (above the 30° latitude belts) as shown in Figure 6. This peculiar finding has also been identified in Fan *et al.* [2012] in convective clouds when the cloud base temperature is below freezing and in simulations of storm track clouds in Igel *et al.* [2013]. Fan *et al.* [2012] hypothesize that less latent heat is released through convective invigoration when the cloud base is below the freezing temperature of water and the clouds are more susceptible to entrainment drying under relatively higher wind shear conditions. A majority (about 60%) of the convective clouds studied here have cold cloud base temperatures in the extratropics. Furthermore, with the strong influence of the AOD on cloud cover fraction and covariability of this relationship with cloud top height, convective invigoration may not be due to aerosol effects and may be caused by other factors such as meteorology [Gryspeerd *et al.*, 2014].

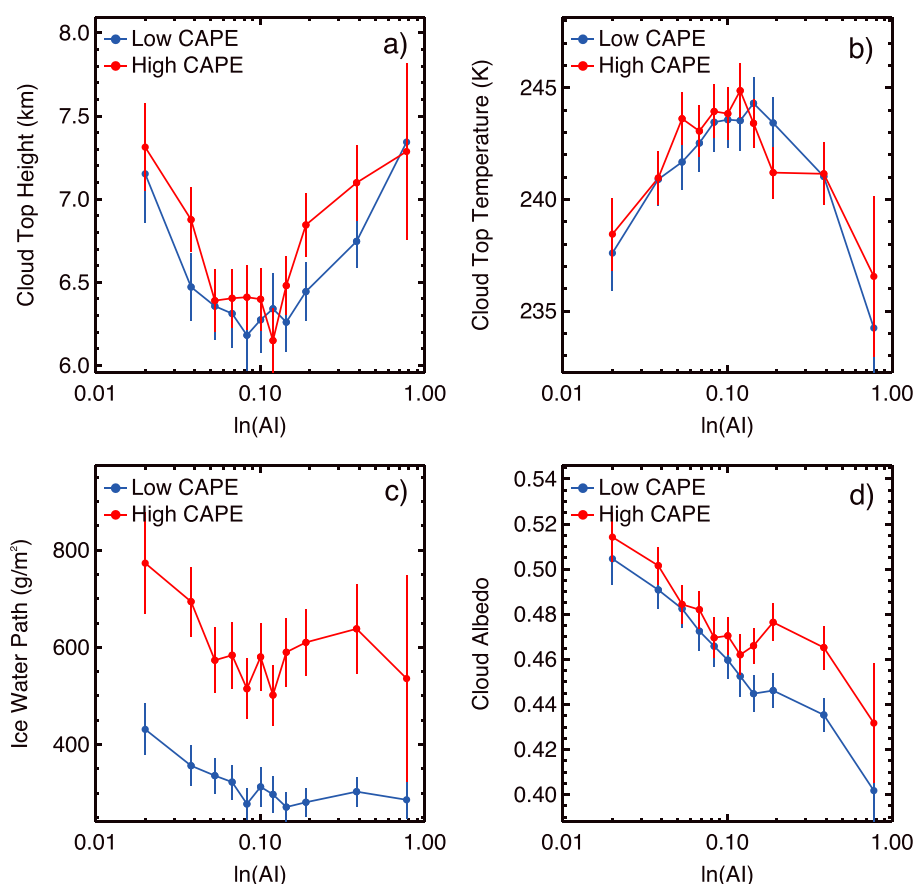


**Figure 6.** Same as Figure 5 except for data extracted from the extratropics (latitude greater than 30°N or latitude less than 30°S).

The proposed hypotheses may explain why the extratropical mixed-phase convective clouds have different susceptibilities to increases in  $AI$  compared to tropical convective clouds. Their contribution to the aerosol indirect effect is substantial and influences the mean sensitivities for global oceanic conditions. For example, the strong negative convective cloud albedo effect in the midlatitudes dominates the global response resulting in a positive shortwave global aerosol indirect forcing (see Figure 3 and Figure S2). Overall, convective clouds impose a net positive aerosol indirect forcing.

### 3.3. Aerosol Indirect Forcing Estimates

Aerosol indirect forcing estimates are provided for each cloud regime in Figure 7 using equations (4) and (5). We find that warm boundary layer clouds exert the single largest control on the net intrinsic aerosol indirect effect, which is estimated to be  $-0.36 \pm 0.21 \text{ W m}^{-2}$  which excludes the impacts due to changes in cloud fraction. The magnitude of this response is in general agreement with other satellite studies of this kind [e.g., *Lebsock et al.*, 2008; *Chen et al.*, 2014]. By including the convective ( $0.15 \pm 0.23 \text{ W m}^{-2}$ ) and cold top boundary layer cloud ( $0.01 \pm 0.06 \text{ W m}^{-2}$ ) composites, the net indirect effect decreases by almost half the value due to the compensating indirect effect sensitivities. The contribution that warm low-level clouds contribute to the total forcing is large in part due to the high sensitivity of the cloud albedo to increases in  $AI$  and their sheer abundance over the ocean. Radiative effects in these other cloud categories tend to be smaller, in part, because they are less frequent, the cloud albedo effect is smaller for cold low cloud, and the shortwave and longwave indirect effects tend to lead to a net positive forcing in convective clouds. Overall, the net oceanic aerosol indirect forcing is  $-0.20 \pm 0.31 \text{ W m}^{-2}$  when all cloud categories are combined. The list of estimates comprising Figure 7 are provided in Table S1.

### 3.4. Uncertainty Assessment

Estimates of the uncertainty attached to the indirect forcing are assessed using a Monte Carlo method. Here cloud albedo,  $AI$ , and anthropogenic aerosol inputs are randomly perturbed by 1%, 30% (based on the

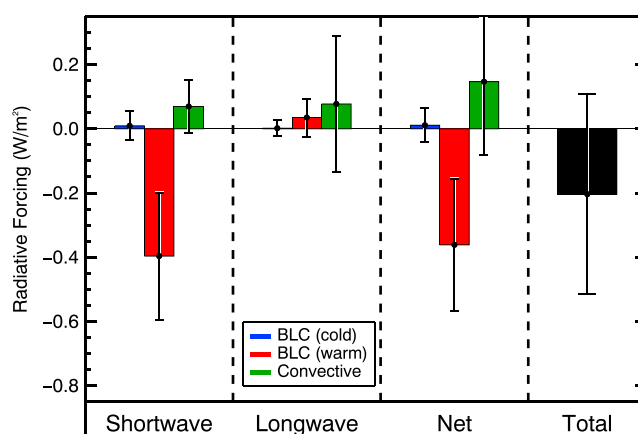


**Figure 7.** Globally averaged oceanic aerosol indirect radiative forcing. Contributions from each cloud category are calculated separately, and the net effect is taken to be the sum of the shortwave and longwave components of the radiative flux and each cloud regime. Error bars, added in quadrature, denote the propagated  $1\sigma$  uncertainty from the observed sensitivity of  $d\alpha/d\ln(AI)$  in equation (2).

validation relationships for aerosol optical depth,  $0.03 + 0.05\tau_a$ , and Ångström exponent), and 16%, respectively. These values are selected based on the measurement uncertainties of the CERES radiative flux measurement [Kato *et al.*, 2010], MODIS-retrieved AOD [Remer *et al.*, 2005] and Ångström exponent [Wagner and Silva, 2008], and MACC-II-retrieved anthropogenic AOD assimilated data [Bellouin *et al.*, 2013]. When the random perturbations are applied the sensitivities of the shortwave and longwave cloud forcing with  $AI$  change and produce a new estimate of the aerosol indirect forcing. After performing these calculations several hundred times using the Monte Carlo method the results are averaged to obtain the uncertainty of  $\pm 0.27 \text{ W m}^{-2}$ . Uncertainties of the intrinsic aerosol-cloud radiative forcing are computed using the standard error of the regression slope based on cloud radiative effect (i.e.,  $\frac{dCRE}{d\ln AI}$ ). Other sources of measurement uncertainty described above are propagated through the calculation of the intrinsic indirect radiative forcing.

Additional assessments are also carried out using MACC-II aerosol index as a proxy for cloud condensation nuclei in Figure S5. One advantage to using MACC-II data is that aerosol optical depth is retrieved in scenes containing high cloud coverage thereby providing more samples for the analysis. However, when using the MACC AOD as the proxy for CCN, we obtain a larger value of the aerosol indirect effect ( $-0.74 \pm 0.71 \text{ W m}^{-2}$ ). Interestingly, the estimate is in better agreement to the satellite-only derived value when the MACC aerosols are sampled outside of the cloudy regions in the same clear-sky locations as MODIS ( $-0.38 \pm 0.47 \text{ W m}^{-2}$ ). Differences in the forcing estimate may be related to a myriad of processes (in the MACC model) including effects related to aerosol particles in clouds by nucleation or impact scavenging, subsequent growth by heterogeneous chemistry and reevaporation, wet scavenging of aerosol particles in particular in areas of strong convection [Grandey *et al.*, 2014; Gryspeerd *et al.*, 2015], aerosol humidification effects [Quaas *et al.*, 2010], and possible errors in data assimilation [Benedetti *et al.*, 2009]. The indirect forcing estimate assessment provided in this paper uses a strictly satellite-based approach to computing aerosol-cloud sensitivities which are convolved with the anthropogenic aerosol fraction as an independent variable in equation (5). Further testing of the algorithms in the MACC-II reanalysis product and satellite data assimilation procedures in multiple cloud regimes is out of the scope of this study but may be needed to constrain these differences against the satellite-only derived sensitivities.

Note that the presented results are based on global oceanic mean sensitivities derived for single-layer clouds for the “whole” of the global oceans. Averaging over this large spatial scale leads to larger uncertainty in the retrieved sensitivities [Grandey and Stier, 2010]. However, by compositing the data into multiple cloud types, a gridded regional analysis approach is not possible due to limited samples residing within each region. Therefore, we examine this approach separately over  $4^\circ \times 4^\circ$  regions in the supporting information, where we find the magnitude of the aerosol indirect effect changes by roughly 15% (see Figure S5).

Separate tests are carried out to quantify the impact of clouds that are assumed not to (or weakly) interact with anthropogenic aerosol. Analysis of additional cloud regimes including all high-level clouds, such as the rest of cirrus and altostratus clouds above 2 km, reveals subtle differences in the overall indirect forcing estimate

compared to using anvil cirrus clouds only in the convective cloud composite. The smaller indirect forcing estimate ( $-0.15 \text{ W m}^{-2}$ ) is due to compensating weaker aerosol-cloud sensitivities in cloud albedo and cloud top height changes despite the large increase in the weighted cloud amount (by including these additional high-level clouds). Nevertheless, we choose not to include them in the overall assessment to ensure that the method targets the effective radiative forcing due to aerosol-cloud interactions. Other physical processes and uncertainties may be introduced by including these clouds, namely, semidirect effects [e.g., Ackerman *et al.*, 2000; Wilcox, 2010], aerosol-radiation interactions affecting clouds via changes in surface solar energetics [Feingold *et al.*, 2005], and effects due to covariability with meteorology.

The construction of equation (2) relies on the assumption that the reflecting surface is dark, like the ocean, where the contribution to all-sky albedo to surface changes is small. This assumption may not be applicable over bright land surfaces or in locations where the clouds are optically thin and transparent to the radiation that is being reflected from the surface. Therefore, we have only provided estimates over the ocean and intend to examine the results for land in a separate study.

#### 4. Conclusions

The rise of anthropogenic aerosol emissions over previous centuries has likely affected the Earth's radiation budget through the modification of cloud properties, although to a highly uncertain extent [IPCC, 2013] due to a poor understanding of aerosol-cloud feedbacks involving ice clouds and a general lack of knowledge regarding preindustrial aerosol sources [e.g., Penner *et al.*, 2011; Carslaw *et al.*, 2013; Ghan *et al.*, 2016]. Here we demonstrate that warm low-level clouds largely influence the strength of the aerosol indirect radiative forcing. However, by incorporating the remaining cloud regimes (convective and cold-topped stratocumulus) with opposing responses to aerosol-cloud relationships, the overall strength of the aerosol indirect forcing decreases. Reasons for this decrease are speculative and hypothesized to involve cloud feedbacks with aerosol that cause shortwave cloud dimming by the glaciation aerosol indirect effect [Lohmann, 2002] in boundary layer clouds and longwave warming by invigoration indirect effect in convective clouds [Rosenfeld *et al.*, 2013].

Results presented here are in general agreement with previous satellite studies which show that an increase in aerosol index enhances cloud albedo and the amount of reflected sunlight from marine warm boundary layer clouds. Given the abundance and strong ocean mean sensitivities to changes in aerosol concentration, it is not surprising that warm low-level clouds dictate the strength of the aerosol indirect effect. What is surprising is that aerosol influences the sum of cold boundary layer clouds and convective cloud regimes to such an extent that a net positive warming effect occurs. Digging into the physics behind these cloud processes is an active area of research. It is likely that aerosols enhance precipitation in mixed-phase clouds [Christensen *et al.*, 2014] thereby causing them to lose total water amount and dim via the glaciation aerosol indirect effect. In convective clouds, an increase in aerosol burden invigorates convection causing the cloud tops to rise and block more of the outgoing longwave radiation to space thereby causing a longwave warming effect on the surface. By extending the radiative forcing calculation from warm low-level clouds to other mixed-phase cloud regimes, the net aerosol indirect effect diminishes by approximately half its estimated value from  $-0.36 \pm 0.21 \text{ W m}^{-2}$  for warm stratocumulus clouds to  $-0.20 \pm 0.31 \text{ W m}^{-2}$  for all combined cloud categories.

The Effective Radiative Forcing for aerosol cloud interactions ( $\text{ERF}_{\text{aci}}$ ) concept was introduced in the IPCC Fifth Assessment Report [IPCC, 2013] to account for the whole range of timescale variability from instantaneous cloud albedo effects to rapid-scale adjustments in cloud lifetime. Representing both of these processes using the slope method between aerosols and cloud properties remains a challenge using satellite data [McComiskey and Feingold, 2012]. There are numerous influences that can also "buffer" [Stevens and Feingold, 2009] cloud responses to increasing aerosol concentration, and these may include dynamical factors associated with cloud field structures, precipitation states, and environmental conditions (to name a few). Using the ubiquitous marine low cloud type, Chen *et al.* [2014] illustrated how different meteorological environments and precipitation states affect cloud liquid water path response and  $\text{ERF}_{\text{aci}}$ . In this work we focus on estimates of aerosol indirect radiative forcing for numerous disparate cloud types, including mixed-phase clouds, convective clouds, and cumulus. Unfortunately, subdividing each cloud type further by environmental and precipitation states does not provide sufficient samples for a robust assessment and is therefore beyond the realm of this work. As satellite sensors continue to accumulate data and more accurate observations become available (e.g., high-resolution broadband radiometer and Doppler radar on EarthCare) we will have new opportunities to untangle the intricate processes making up the highly uncertain estimate of  $\text{ERF}_{\text{aci}}$ .

Overall, the results from this study suggest that aerosol effects on clouds depend on the cloud state and that mixed-phase cloud regimes may buffer part of the strong cooling response that aerosols have on warm boundary layer clouds. While it is not considered here, aerosol effects on spreading anvils (i.e., anvils further away from convective cores than considered here) may cause even greater warming and stronger buffering to the net indirect effect than can be shown with this data set. It is therefore imperative to consider all major cloud categories, particularly mixed-phase clouds, in estimates of the global aerosol indirect forcing.

## Acknowledgments

We thank the anonymous reviewers for their insightful and constructive comments in assessing the quality of this research. We thank NASA Goddard (<https://ladsweb.nascom.nasa.gov>) for MODIS data, NASA Langley for CCCM data (<http://ceres.larc.nasa.gov>), the Cooperative Institute for Research in the Atmosphere for CloudSat data (<http://www.cloudsat.cira.colostate.edu>), and NASA Atmospheric Science Data Center for CALIPSO data (<https://eosweb.larc.nasa.gov/>) used in this paper. Part of the research was carried out at CSU under NASA grant NASS-99237 and NSF award AGS-0968648 "Collaborative Research: Cloud Macrophysical Parameterization and its Application to Aerosol Indirect Effect", with the other portion at JPL, Caltech, under a contract with NASA funded by grant NNN13D771T and JPL CloudSat subcontract 1439268.

## References

- Ackerman, A. S., O. B. Toon, D. E. Stevens, A. J. Heymsfield, V. Ramanathan, and E. J. Welton (2000), Reduction of tropical cloudiness by soot, *Science*, *12*, 1042–1047.
- Ackerman, A. S., M. P. Kirkpatrick, D. E. Stevens, and O. B. Toon (2004), The impact of humidity above stratiform clouds on indirect aerosol climate forcing, *Nature*, *432*, 1014–1017, doi:10.1038/nature03174.
- Albrecht, B. A. (1989), Aerosols, cloud microphysics, and fractional cloudiness, *Science*, *245*, 1227–1230.
- Alterskjær, K., J. E. Kristjánsson, and C. Hoese (2010), Do anthropogenic aerosols enhance or suppress the surface cloud forcing in the Arctic?, *J. Geophys. Res.*, *115*, D22204, doi:10.1029/2010JD014015.
- Anderson, T. L., R. J. Charlson, D. M. Winker, J. A. Ogren, and K. Holmén (2003), Mesoscale variations of tropospheric aerosols, *J. Atmos. Sci.*, *60*(1), 119–136, doi:10.1175/1520-0469(2003)060<0119:MVOTA>2.0.CO;2.
- Belloquin, N., J. Quaas, J.-J. Morcrette, and O. Boucher (2013), Estimates of aerosol radiative forcing from the MACC re-analysis, *Atmos. Chem. Phys.*, *13*(4), 2045–2062, doi:10.5194/acp-13-2045-2013.
- Benedetti, A., et al. (2009), Aerosol analysis and forecast in the European Centre for Medium-Range Weather Forecasts Integrated Forecast System: 2. Data assimilation, *J. Geophys. Res.*, *114*, D13205, doi:10.1029/2008JD011115.
- Bennartz, R. (2007), Global assessment of marine boundary layer cloud droplet number concentration from satellite, *J. Geophys. Res.*, *112*, D02201, doi:10.1029/2006JD007547.
- Borys, R. D., D. H. Lowenthal, S. A. Cohn, and W. O. J. Brown (2003), Mountaintop and radar measurements of anthropogenic aerosol effects on snow growth and snowfall rate, *Geophys. Res. Lett.*, *30*(10), 1538, doi:10.1029/2002GL016855.
- Carlsaw, K. S., et al. (2013), Large contribution of natural aerosols to uncertainty in indirect forcing, *Nature*, *503*, 67–71, doi:10.1038/nature12674.
- Chen, Y.-C., M. W. Christensen, G. L. Stephens, and J. H. Seinfeld (2014), Satellite-based estimate of global aerosol-cloud radiative forcing by marine warm clouds, *Nat. Geosci.*, *7*(8), 643–646, doi:10.1038/ngeo2214.
- Christensen, M. W., G. L. Stephens, and M. D. Lebsock (2013), Exposing biases in retrieved low cloud properties from CloudSat: A guide for evaluating observations and climate data, *J. Geophys. Res. Atmos.*, *118*, 12,120–12,131, doi:10.1002/2013JD020224.
- Christensen, M. W., K. Suzuki, B. Zambri, and G. L. Stephens (2014), Ship track observations of a reduced shortwave aerosol indirect effect in mixed-phase clouds, *Geophys. Res. Lett.*, *41*, 6970–6977, doi:10.1002/2014GL061320.
- Coakley, J. (1979), A study of climate sensitivity using a simple energy balance model, *J. Atmos. Sci.*, *36*(2), 260–269, doi:10.1175/1520-0469(1979)036<0260:ASOCSU>2.0.CO;2.
- Fan, J., T. Yuan, J. M. Comstock, S. Ghan, A. Khain, L. R. Leung, Z. Li, V. J. Martins, and M. Ovchinnikov (2009), Dominant role by vertical wind shear in regulating aerosol effects on deep convective clouds, *J. Geophys. Res.*, *114*, D22206, doi:10.1029/2009JD012352.
- Fan, J., D. Rosenfeld, Y. Ding, L. R. Leung, and Z. Li (2012), Potential aerosol indirect effects on atmospheric circulation and radiative forcing through deep convection, *Geophys. Res. Lett.*, *39*, L09806, doi:10.1029/2012GL051851.
- Fan, J., L. R. Leung, D. Rosenfeld, Q. Chen, Z. Li, J. Zhang, and H. Yan (2013), Microphysical effects determine macrophysical response for aerosol impacts on deep convective clouds, *Proc. Natl. Acad. Sci. U.S.A.*, *110*(48), E4581–E4590, doi:10.1073/pnas.1316830110.
- Feingold, G., G. H. Jiang, and J. Y. Harrington (2005), On smoke suppression of clouds in Amazonia, *Geophys. Res. Lett.*, *32*, L02804, doi:10.1029/2004GL021369.
- Fu, Q., and K. N. Liou (1993), Parameterization of the radiative properties of cirrus clouds, *J. Atmos. Sci.*, *50*(13), 2008–2025, doi:10.1175/1520-0469(1993)050<2008:POTRPO>2.0.CO;2.
- Garrett, T. J., L. F. Radke, and P. V. Hobbs (2002), Aerosol effects on cloud emissivity and surface longwave heating in the Arctic, *J. Atmos. Sci.*, *59*(3), 769–778, doi:10.1175/1520-0469(2002)059<0769:AEOCEA>2.0.CO;2.
- Ghan, S., et al. (2016), Challenges in constraining anthropogenic aerosol effects on cloud radiative forcing using present-day spatiotemporal variability, *Proc. Natl. Acad. Sci. U. S. A.*, *113*(21), 5804–5811, doi:10.1073/pnas.1514036113.
- Golaz, J.-C., L. W. Horowitz, and H. Levy (2013), Cloud tuning in a coupled climate model: Impact on 20th century warming, *Geophys. Res. Lett.*, *40*, 2246–2251, doi:10.1002/grl.50232.
- Grandey, B. S., and P. Stier (2010), A critical look at spatial scale choices in satellite-based aerosol indirect effect studies, *Atmos. Chem. Phys.*, *10*(23), 11,459–11,470, doi:10.5194/acp-10-11459-2010.
- Grandey, B. S., P. Stier, and T. M. Wagner (2013), Investigating relationships between aerosol optical depth and cloud fraction using satellite, aerosol reanalysis and general circulation model data, *Atmos. Chem. Phys.*, *13*(6), 3177–3184, doi:10.5194/acp-13-3177-2013.
- Grandey, B. S., A. Gururaj, P. Stier, and T. M. Wagner (2014), Rainfall-aerosol relationships explained by wet scavenging and humidity, *Geophys. Res. Lett.*, *41*, doi:10.1002/2014GL060958.
- Gryspeerdt, E., P. Stier, and B. S. Grandey (2014), Cloud fraction mediates the aerosol optical depth-cloud top height relationship, *Geophys. Res. Lett.*, *41*, 3622–3627, doi:10.1002/2014GL059524.
- Gryspeerdt, E., P. Stier, B. A. White, and Z. Kipling (2015), Wet scavenging limits the detection of aerosol effects on precipitation, *Atmos. Chem. Phys.*, *15*, 7557–7570, doi:10.5194/acp-15-7557-2015.
- Gryspeerdt, E., J. Quaas, and N. Bellouin (2016), Constraining the aerosol influence on cloud fraction, *J. Geophys. Res. Atmos.*, *121*, 3566–3583, doi:10.1002/2015JD023744.
- Haynes, J. M., T. S. L'Ecuyer, G. L. Stephens, S. D. Miller, C. Mitrescu, N. B. Wood, and S. Tanelli (2009), Rainfall retrieval over the ocean with spaceborne W-band radar, *J. Geophys. Res.*, *114*, D00A22, doi:10.1029/2008JD009973.
- Igel, A. L., S. C. van den Heever, C. M. Naud, S. M. Saleeby, and D. J. Posselt (2013), Sensitivity of warm-frontal processes to cloud-nucleating aerosol concentrations, *J. Atmos. Sci.*, *70*(6), 1768–1783, doi:10.1175/JAS-D-12-0170.1.
- Intergovernmental Panel on Climate Change (IPCC) (2007), Summary for policymakers, in *Climate Change 2007: The Physical Science Basis. Contribution of Working Group I to the Fourth Assessment Report of the Intergovernmental Panel on Climate Change*, edited by S. Solomon et al., Cambridge Univ. Press, Cambridge, U. K., and New York.



- Intergovernmental Panel on Climate Change (IPCC) (2013), Summary for policymakers, in *Climate Change 2013: The Physical Science Basis, Contribution of Working Group I to the Fifth Assessment Report of the Intergovernmental Panel on Climate Change*, edited by T. F. Stocker, D. Qin, and G. Plattner, Cambridge Univ. Press, Cambridge, U. K., and New York.
- Jin, Z., Y. Qiao, Y. Wang, Y. Fang, and W. Yi (2011), A new parameterization of spectral and broadband ocean surface albedo, *Opt. Express*, 19(27), 26,429–26,443, doi:10.1364/OE.19.026429.
- Kato, S., S. Sun-Mack, W. F. Miller, F. G. Rose, Y. Chen, P. Minnis, and B. A. Wielicki (2010), Relationships among cloud occurrence frequency, overlap, and effective thickness derived from Calipso and CloudSat merged cloud vertical profiles, *J. Geophys. Res.*, 115, D00H28, doi:10.1029/2009JD012277.
- Kato, S., et al. (2011), Improvements of top-of-atmosphere and surface irradiance computations with Calipso-, CloudSat-, and MODIS-derived cloud and aerosol properties, *J. Geophys. Res.*, 116, D19209, doi:10.1029/2011JD016050.
- Kaufman, Y. J., I. Koren, L. A. Remer, D. Rosenfeld, and Y. Rudich (2005), The effect of smoke, dust, and pollution aerosol on shallow cloud development over the Atlantic Ocean, *Proc. Natl. Acad. Sci. U.S.A.*, 102(32), 11,207–11,212, doi:10.1073/pnas.05051911102.
- Khain, A. P. (2009), Notes on state-of-the-art investigations of aerosol effects on precipitation: A critical review, *Environ. Res. Lett.*, 4(1), 015004, doi:10.1088/1748-9326/4/1/015004.
- Koren, I., G. Feingold, and L. A. Remer (2010), The invigoration of deep convective clouds over the Atlantic: Aerosol effect, meteorology or retrieval artifact?, *Atmos. Chem. Phys.*, 10(18), 8855–8872, doi:10.5194/acp-10-8855-2010.
- Lebsock, M. D., G. L. Stephens, and C. Kummerow (2008), Multisensor satellite observations of aerosol effects on warm clouds, *J. Geophys. Res.*, 113, D15205, doi:10.1029/2008JD009876.
- Li, J., J. Huang, K. Stamnes, T. Wang, Q. Lv, and H. Jin (2015), A global survey of cloud overlap based on Calipso and CloudSat measurements, *Atmos. Chem. Phys.*, 15(1), 519–536, doi:10.5194/acp-15-519-2015.
- Loeb, N., B. Wielicki, D. Doelling, G. Smith, D. Keyes, S. Kato, N. Manalo-Smith, and T. Wong (2009), Toward optimal closure of the Earth's top-of-atmosphere radiation budget, *J. Clim.*, 22, 748–766, doi:10.1175/2008JCLI2637.1.
- Lohmann, U. (2002), A glaciation indirect aerosol effect caused by soot aerosols, *Geophys. Res. Lett.*, 29(4), 1052, doi:10.1029/2001GL014357.
- McComiskey, A., and G. Feingold (2012), The scale problem in quantifying aerosol indirect effects, *Atmos. Chem. Phys.*, 12(2), 1031–1049, doi:10.5194/acp-12-1031-2012.
- Morcrette, J.-J., et al. (2009), Aerosol analysis and forecast in the European Centre for Medium-Range Weather Forecasts Integrated Forecast System: Forward modeling, *J. Geophys. Res.*, 114, D06206, doi:10.1029/2008JD011235.
- Nakajima, T., A. Higurashi, K. Kawamoto, and J. E. Penner (2001), A possible correlation between satellite-derived cloud and aerosol microphysical parameters, *Geophys. Res. Lett.*, 28(7), 1171–1174, doi:10.1029/2000GL012186.
- Penner, J. E., L. Xu, and M. Wang (2011), Satellite methods underestimate indirect climate forcing by aerosols, *Proc. Natl. Acad. Sci. U.S.A.*, 108(33), 13,404–13,408, doi:10.1073/pnas.1018526108.
- Pincus, R., and M. B. Baker (1994), Effect of precipitation on the albedo susceptibility of clouds in the marine boundary layer, *Nature*, 372, 250–252.
- Pueschel, R. F., J. Hallett, A. W. Strawa, S. D. Howard, and G. V. Ferry (1997), Aerosol and cloud particles in tropical cirrus anvil: Importance to radiation balance, *J. Aerosol Sci.*, 28, 1123–1136.
- Quaas, J., O. Boucher, N. Bellouin, and S. Kinne (2008), Satellite-based estimate of the direct and indirect aerosol climate forcing, *J. Geophys. Res.*, 113, D05204, doi:10.1029/2007JD008962.
- Quaas, J., B. Stevens, P. Stier, and U. Lohmann (2010), Interpreting the cloud cover-aerosol optical depth relationship found in satellite data using a general circulation model, *Atmos. Chem. Phys.*, 10, 6129–6135, doi:10.5194/acp-10-6129-2010.
- Remer, L. A., et al. (2005), The MODIS aerosol algorithm, products, and validation, *J. Atmos. Sci.*, 62(4), 947–973, doi:10.1175/JAS3385.1.
- Rosenfeld, D., U. Lohmann, G. B. Raga, C. D. O'Dowd, M. Kulmala, S. Fuzzi, A. Reissell, and M. O. Andreae (2008), Flood or drought: How do aerosols affect precipitation?, *Science*, 321(5894), 1309–1313, doi:10.1126/science.1160606.
- Rosenfeld, D., R. Wood, L. J. Donner, and S. C. Sherwood (2013), Aerosol cloud-mediated radiative forcing: Highly uncertain and opposite effects from shallow and deep clouds, in *Climate Science for Serving Society*, edited by G. R. Asrar and J. W. Hurrell, pp. 105–149, Springer, Netherlands.
- Sorooshian, A., G. Feingold, M. D. Lebsock, H. Jiang, and G. L. Stephens (2009), On the precipitation susceptibility of clouds to aerosol perturbations, *Geophys. Res. Lett.*, 36, L13803, doi:10.1029/2009GL038993.
- Stephens, G. L., P. M. Gabriel, and S. C. Tsay (1991), Statistical radiative transport in one-dimensional media and its application to the terrestrial atmosphere, *Transp. Theory Stat. Phys.*, 20, 139–175, doi:10.1080/00411459108203900.
- Stevens, B., and G. Feingold (2009), Untangling aerosol effects on clouds and precipitation in a buffered system, *Nature*, 461, 607–613, doi:10.1038/nature08281.
- Storer, R. L., S. C. van den Heever, and T. S. L'Ecuyer (2014), Observations of aerosol-induced convective invigoration in the tropical east Atlantic, *J. Geophys. Res. Atmos.*, 119, 3963–3975, doi:10.1002/2013JD020272.
- Twomey, S. (1974), Pollution and the planetary albedo, *Atmos. Environ.*, 8, 1251–1256.
- Wagner, F., and M. Silva (2008), Some considerations about Angstrom exponent distributions, *Atmos. Chem. Phys.*, 8, 481–489, doi:10.5194/acp-8-481-2008.
- Wang, Z., and K. Sassen (2001), Cloud type and macrophysical property retrieval using multiple remote sensors, *J. Appl. Meteorol.*, 40(10), 1665–1682, doi:10.1175/1520-0450(2001)040<1665:CTAMPR>2.0.CO;2.
- Wilber, A. C., D. P. Kratz, and S. K. Gupta, (1999), Surface emissivity maps for use in satellite retrievals of longwave radiation, Tech. Memo. NASA/TP- 1999-209362, NASA, Washington, D. C.
- Wilcox, E. M. (2010), Stratocumulus cloud thickening beneath layers of absorbing smoke aerosol, *Atmos. Chem. Phys. Discuss.*, 10(8), 18,635–18,659, doi:10.5194/acpd-10-18635-2010.
- Wood, R. (2012), Stratocumulus clouds, *Mon. Weather Rev.*, 140, 2,373–2,423, doi:10.1175/MWR-D-11-00121.1.
- World Meteorological Organization (1956), *International Cloud Atlas: Abridged Atlas*, 62 pp., World Meteorol. Organ., Geneva.